https://doi.org/10.26599/FRICT.2026.9441314

Research Article

Cilia-inspired hydrogel surfaces for low-pressure lubrication via interfacial water structuring

Yixiao Wang[1,3], Peijia Li[1,3], Yilin Wang[1,3], Zhaoxiang Lu[2], Yun Feng[*2]✉, Ye Tian[*1,3]✉, Lei Jiang[1,3,4]

[1] Laboratory of Bio-Inspired Materials and Interface Sciences, Technical Institute of Physics and Chemistry, Chinese Academy of Sciences, Beijing 100190, China.

[2] Department of Ophthalmology, Peking University First Hospital, Beijing 100034, China.

[3] School of Future Technology, University of Chinese Academy of Sciences, Beijing 100049, China.

[4] Suzhou Institute for Advanced Research, University of Science and Technology of China, Suzhou 215123, China.

✉ Corresponding author. E-mail: tianyely@iccas.ac.cn; fengyun@bjmu.edu.cn

Received: March 31, 2026; Revised: June 10, 2026; Accepted: September 7, 2026

Abstract: Lubrication plays a vital role in flexible electronics and medical devices, yet achieving stable low friction under low-pressure hydrodynamic conditions remains challenging. Existing approaches often lead to a coefficient of friction (COF) that increases with sliding velocity, due to the instability of interfacial water layers. Inspired by ocular surface structures, we developed a bio-inspired lubricating hydrogel (BLH) with nanowire arrays that confine interfacial water. This confined water remains stable under pressure, allowing COF to stay low and nearly independent of velocity. Under eyelid pressure (1.3-7.0 kPa), BLH achieved an ultra-low COF (0.0079-0.028), representing a 34-80% reduction

compared to flat hydrogels (FH) and approaching that of natural corneal surfaces (0.014-0.037). The low friction was sustained over prolonged durations (≈ 6,000 s) and maintained at blinking-relevant speeds (≈ 4 cm/s). Tests using pig-eyeball rubbing and endoscope-probe models further demonstrated the robustness of this strategy, highlighting its promise for low-hysteresis coatings, flexible electronics, and medical devices.

Keywords: hydrogel, confined interfacial water, lubrication, nanowire, bio-inspired materials

1 Introduction

Reducing friction and wear at the interface is critical for a wide range of applications in engineering [1,2], life sciences [3,4], and medicine [5,6]. Understanding lubrication mechanisms is essential for designing efficient materials for medical devices [7-9], flexible electronics [10-12], and other technologies [13-15]. Inspired by biological systems, significant progress has been made in boundary lubrication, particularly under high pressures where interfacial forces dominate and hydration layers can reduce shear stress between interfaces [16–19]. However, these strategies are less effective in low-pressure hydrodynamic regimes (experimental range: 1.3–25.0 kPa), where surfaces are separated by a liquid film and friction is governed by the structural properties of interfacial water rather than by direct solid-solid interactions [20–22]. In such low-pressure environments-typical of flexible electronics [23] and biomedical devices [24-26] -maintaining stable, ultra-low friction remains challenging. The instability of interfacial water layers under dynamic sliding often leads to increased friction with velocity, limiting the durability and responsiveness of these systems. Developing lubrication strategies that stabilize water-mediated interfaces under weak confinement pressure is thus a key frontier in tribology.

Ocular surfaces provide an efficient natural solution to low-pressure lubrication. The tear film, dominated by its aqueous layer, maintains separation between the cornea and the eyelid conjunctiva, enabling smooth motion under physiologically relevant eyelid pressures. Although some studies have

explored improving tear-film lubrication by supplementing with external agents [27-29], the fundamental role of interfacial water structure has received little attention. In particular, how surface microstructures, such as corneal and conjunctival cilia, regulate water organization at the interface to achieve ultra-low friction remains poorly understood.

Inspired by ocular surface structures, we developed a bio-inspired lubricating hydrogel (BLH) featuring nanowire arrays that regulate interfacial water behavior. These nanowires stabilize the aqueous layer at the interface under physiologically relevant eyelid pressures (1.3-7.0 kPa), allowing BLH to achieve an ultra-low, velocity-independent COF of 0.0079-0.028, corresponding to a 34-80% reduction relative to flat hydrogels (FH) and approaching that of natural corneal surfaces (0.014-0.037). The low friction was maintained over prolonged durations (≈ 6,000 s) and at blinking-relevant speeds (≈ 4 cm/s). In realistic tests, including pig-eye rubbing and endoscope-probe models, BLH significantly mitigated surface damage and reduced motion hysteresis, highlighting its potential as a robust, low-hysteresis coating for biomedical devices and flexible electronics operating under low-pressure lubrication.

2 Results and discussion

2.1 Friction behavior of biological and bio-inspired surfaces

During physiological blinking, the eyelid smoothly traverses the convex corneal surface, generating remarkably low frictional resistance while transmitting axial forces (Fig. 1a). Nanostructural characterization reveals critical differences between healthy and pathological ocular surfaces: healthy corneas display intact architectural features (Fig. 1b), whereas vertically aligned ciliary microstructures are disrupted in dry eye disease (DED)-affected specimens (Fig. 1c). Inspired by cilia structure on heathy cornea and damaged cilia structure on DED cornea (Fig. 1d), we fabricated BLH and FH, respectively, to investigate the mechanism of lubricating under weak pressure.

Surface morphological analysis through scanning electron microscopy (SEM) demonstrated clear contrasts: BLH exhibited well-ordered nanowire arrays with defined dimensions (diameter ≈ 90 nm, length ≈ 1 μm; Fig. 1e) while unstructured FH showed featureless surfaces (Fig. 1f). Systematic

fabrication produced 16 hydrogel variants with nanowire diameters ranging 90-400 nm and lengths spanning 1-4 μm, designated BLH1 through BLH16 in a combinatorial scheme (Fig. S1).

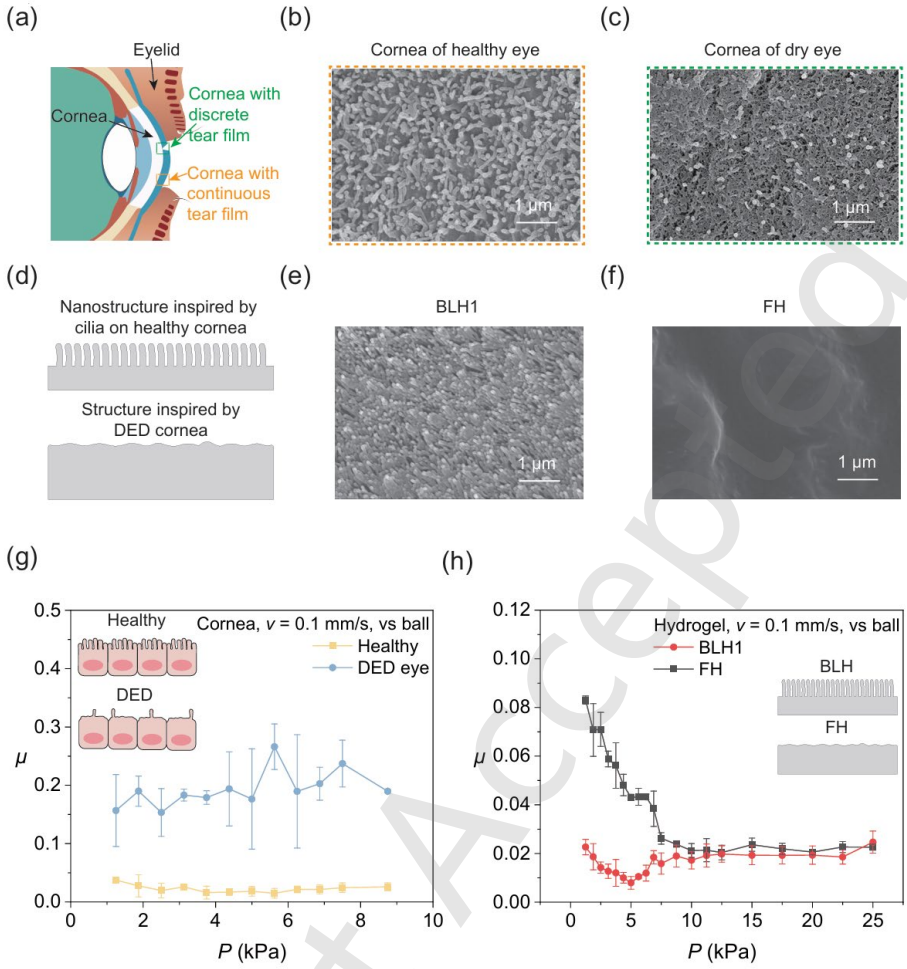

Fig 1. Surface morphology of cornea and hydrogel, and corresponding friction measurements. (a) Schematic illustration of ocular surface under eyelid pressure during blinking. Continuous tear film exists between healthy cornea and eyelid, and discrete tear film exists between dry eye cornea and eyelid. (b) Morphology of healthy cornea (dense cilia). (c) Morphology of dry eye cornea (sparse and damaged cilia). (d) Schematic of structures inspired by cilia on healthy cornea and DED cornea. (e) SEM images of BLH1 with nanowires (diameter ≈ 90 nm, length ≈ 1 μm). (f) SEM images of unstructured FH. (g) Comparison of healthy and DED cornea friction with steel ball under eyelid pressure. (h) Comparison of BLH1 and FH friction with steel ball. Error bars represent 3 parallel samples.

To evaluate the functional relevance of artificial cilia, COF measurements were performed between corneal surfaces and a polished steel sphere (bought from Bruker) (Fig.S2) under physiologically relevant pressures (1.3-8.8 kPa) at a sliding velocity of 0.1 mm/s. We measured the contact area of steel ball and hydrogel by the fluorescent nanoparticles and the contact area was about 8 mm^2 (Fig.S3). Deionized water (DI water) lubrication was used to isolate structural effects from mucin-mediated contributions. As shown in Fig. 1g, quantitative analysis revealed substantial friction differences: DED corneas exhibited elevated COF values (0.15-0.23), contrasting sharply with healthy corneal surfaces (0.014-0.037). Notably, the low COF observed in healthy specimens under aqueous lubrication align closely with published clinical benchmarks [30-32], experimentally confirming the critical role of intact cilia.

COF measurements across the full experimental pressure range (1.3–25.0 kPa) at a sliding velocity of 0.1 mm/s revealed the lubrication performance of BLH1 and FH (Fig. 1h). FH exhibited a rapid decrease in COF from 1.3 to 7.5 kPa, followed by stabilized oscillatory behavior at 7.5-25.0 kPa. In contrast, BLH1 showed triphasic behavior: a gradual friction decrease (1.3-5.0 kPa), a subtle increase (5.0-7.0 kPa), and subsequent stabilization (7.0-25.0 kPa), with minimal COF (0.0079) observed at 5.0 kPa. This pressure threshold corresponds to the transition into optimal hydrodynamic lubrication conditions.

To elucidate the fundamental mechanisms underlying the pressure dependent frictional responses of BLH1 and FH surfaces, we employed a multiscale investigation combining macroscopic tribological tests with nanoscale analysis of interfacial water structure.

2.2 Macroscale friction behavior

We systematically evaluated the COF for the BLH1-BLH16 series under progressive increasing pressures (1.3-25.0 kPa) at 0.1 mm/s (Fig. 2a and Fig. S4). Three distinct friction phases were observed and emphasized with colors in Fig. 2a: an initial gradual COF decline, a moderate increase and subsequent stabilized oscillations. Besides, as is shown in Fig. 2b, the pressure at which the COF

reached its minimum decreased with increasing nanowire length, suggesting that longer nanowire undergo progressive deformation at lower pressures.

The classical Stribeck curve describes lubrication state transitions through the dimensionless Hersey number:

$$Hr = \frac{\eta v}{P} \quad (1)$$

where *Hr* is Hersey number, η is the viscosity of lubricant, and *v* and *P* are the friction speed and applied pressure, respectively [33].

In boundary lubrication, persistent surface passivation maintains stable asperity contact, resulting in velocity independent COF, while in hydrodynamic lubrication, the formation of aqueous films generates sufficient hydrodynamic lift to fully separate the surfaces, as evidenced by the COF's linear dependence on sliding velocity [34]. Consequently, the velocity dependence of friction directly reflects the contact dynamics at the interfaces and simultaneously characterizes the lubrication stability and load bearing capacity of the interfacial water film.

To determine the lubrication regime of BLH, comparative tribological analyses were performed under controlled interfacial conditions. Because BLH1 has more obvious and more easily observable trends than BLH2-BLH4 and lower COF than BLH5-BLH16, it was selected as a representative example. As is shown in Fig. 2c, dry BLH1 surfaces under baseline conditions (4.0 kPa, 0.1 mm/s) exhibited a progressive increase in COF over 600 s, with corresponding nanowire fracture patterns (Fig. 2c inset). Conversely, for hydrated BLH1 systems, measurements at the upper end of the experimental pressure range (25.0 kPa) and minimal sliding velocity (0.1 mm/s) revealed a stable COF ($\mu \approx 0.031$) maintained over 6,000 s, with the nanowire array remaining intact (Fig. 2d inset).This behavior is consistent with Bernoulli's principle for thin-film hydrodynamics, where low velocity at constant pressure reduces hydrodynamic lift. The contrast in wear morphology and temporal stability conclusively demonstrates hydrodynamic lubrication dominance in water environments, where pressurized liquid films maintain complete surface separation throughout the tested parameter space.

To conclusively establish the hydrodynamic lubrication regime, we systematically measured the COF of BLH1 and FH across a pressure range of 4.4-25.0 kPa and sliding velocities spanning 0.1-38.0 mm/s (Fig. 2e). The FH samples exhibited a consistent positive correlation between COF and sliding velocity across all pressure conditions. In contrast, BLH1 demonstrated distinct pressure dependent behavior: below critical pressure thresholds (4.4-5.0 kPa), its COF displayed velocity dependence with comparable slopes to FH. However, when subjected to higher pressures (>5.6 kPa), BLH1's COF exhibited nearly velocity-independent. Notably, the transition pressure of 5.0 kPa coincided with the minimum COF observed in BLH1. As interfacial water is the key factor in hydrodynamic lubrication, we further investigate and compare the difference of interfacial water between BLH and FH from micro level.

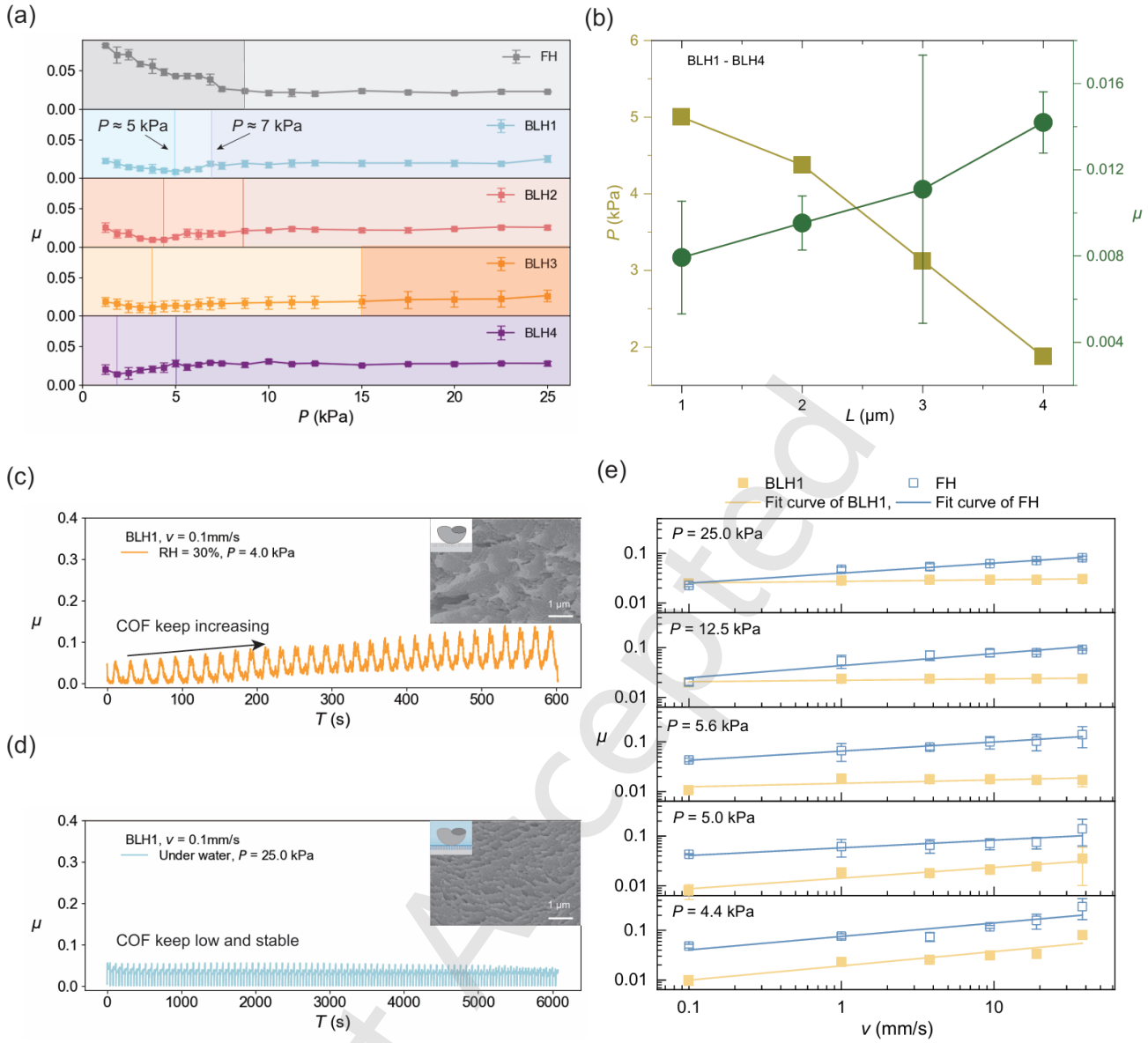

Fig 2. Performance of friction under various pressures and velocities at macroscale. (a) Plots of BLH1–4 and FH friction performance under different pressures. (b) Pressure vs nanowire length at minimum point of COF of BLH1-4. (c) Data plots of μ-t curves of BLH1 under 4.0 kPa (RH 30%) in about 600 s and the nanowire morphology after friction. (d) Data plots of μ-t curves of BLH1 under 25.0 kPa under water in over 6000 s and the nanowire morphology after wear. (e) Graphs of μ vs velocity for BLH1 and FH under pressures 4.4, 5.0, 5.6, 12.5, and 25.0 kPa at speeds 0.1, 1.0, 3.8, 9.4, 19.0, and 38.0 mm/s. All error bars represent at least 3 parallel samples.

2.3 Interfacial water structure at microscale

To systematically investigate structural distinctions between BLH1's confined interfacial water and FH's interfacial water, attenuated total reflection infrared (ATR-IR) spectroscopy, low-field nuclear magnetic resonance (LF-NMR), and Differential scanning calorimetry (DSC) were strategically combined to probe water organization at microscale.

We performed attenuated total reflection infrared (ATR-IR) analysis of interfacial water organization on hydrogel surfaces. The broad band of vibrational spectrum of water between 2,800 and 4,000 cm^{-1} could be deconvoluted into three peaks centered at about 3,600, 3,400 and 3,200 cm^{-1}, in which the peak at 3,200 cm^{-1} indicates strongly bound water molecules with tetrahedral structure (ice-like water) and the peaks at 3,400 cm^{-1} and 3,600 cm^{-1} are attributed to the incomplete tetrahedral coordination (asymmetric water) and free state associated with non-hydrogen-bonded OHs, respectively [35].

Ice-like water organizes into structured molecular layers on solid surfaces through robust hydrogen-bond networks. This structural ordering enhances molecular cohesion, necessitating greater shear forces to initiate sliding motion and consequently elevating frictional resistance. Furthermore, the intense hydrogen-bonding interactions between ice-like water molecules amplify interfacial adhesion forces. Nanowire array confinement disrupts hydrogen-bond orientation, inducing randomized spatial distribution within constrained water domains. Molecular interactions between water and nanostructures promote molecular reorientation, diminishing hydrogen-bond directionality [36,37]. This structural disordering directly modulates frictional behavior through altered interfacial energetics. We compared the ATR-IR spectrum of BLH1 and FH in Fig. S6a: BLH1 surfaces have more asymmetric water and less tetrahedral water than FH surfaces. Correspondingly, COF of BLH1 is lower than that of FH under 3.0 kPa.

To systematically investigate pressure-induced water state transitions and interfacial water film component reorganization, we conducted in situ ATR-IR spectroscopic measurements under precisely controlled pressure conditions (3.0-25.0 kPa) with integrated load monitoring via a handheld

dynamometer and the loads were calculated (Fig.S5).. Experiments on highly oriented pyrolytic graphite (HOPG) confirmed that water structural modifications are pressure-independent (Fig. S6b). Spectral analysis of BLH1 and FH surfaces under dehydrated (0 μL) and hydrated (30 μL) conditions showed that BLH1 exhibits more asymmetric and less tetrahedral interfacial water than FH below 10.0 kPa, whereas both surfaces show similar interfacial water composition above 10.0 kPa, in agreement with their macroscopic friction behavior. Here, we use baseline correction with the 3.0 kPa spectra to clearly visualize pressure-dependent changes in interfacial water components via difference spectrum analysis. As is shown in Fig. 3a and Fig. S6c- Fig. S6f, as to surface-dried hydrogels, FH exhibited progressive decrease in tetrahedral water component, concomitant increase in asymmetric water component and stable free water component, while BLH1 showed stable tetrahedral, asymmetric, and free water components. Fig. 3b shows similar trends of water components change with pressure on both FH and BLH1 surfaces with 30 μL water and Fig. S7 shows the quantitative results to BLH1 surfaces and FH surfaces with 0 and 30 μL water and we can conclude that interfacial water confined on BLH1 surfaces have components more stable than water on FH surfaces.

We also employed low-field nuclear magnetic resonance (LF-NMR) to characterize aqueous molecular mobility at hydrogel interfaces. To preferentially analyze interfacial water while minimizing bulk phase contributions, cryostat microtome-prepared BLH1 and FH samples (3 μm and 50 μm thicknesses, respectively) and normal samples with 1mm thickness were prepared. As illustrated in Fig. 3c, comparing hydrogels of 1 mm, 50 μm, and 3 μm thickness, we observed that peaks at 0.1-1 ms (red region, hydrogel-trapped water) and 1-4 ms (blue region, surface-confined water) increased in amplitude with decreasing thickness, while peaks above 10 ms (orange region, free water) decreased sharply, reflecting an increasing ratio of confined water and a decreasing ratio of free water [38,39]. Moreover, after introducing nanowire array on hydrogel surface, T_2 located in 1-4 ms shifts from 3.3 ms to 2.4 ms, indicating that water molecules on BLH surfaces are bound more tightly than on FH surfaces.

DSC was also used to quantify water states in hydrogels, distinguishing non-freezing (bound) from freezing (bulk-like) water. In BLH, the non-freezing/freezing water ratio (W_n/W_f) rose from 0.2 to 0.6

with chain length extension (Fig. S8 and Fig. S9), confirming stronger water-binding capacity than FH in line with ATR-IR and LF-NMR.

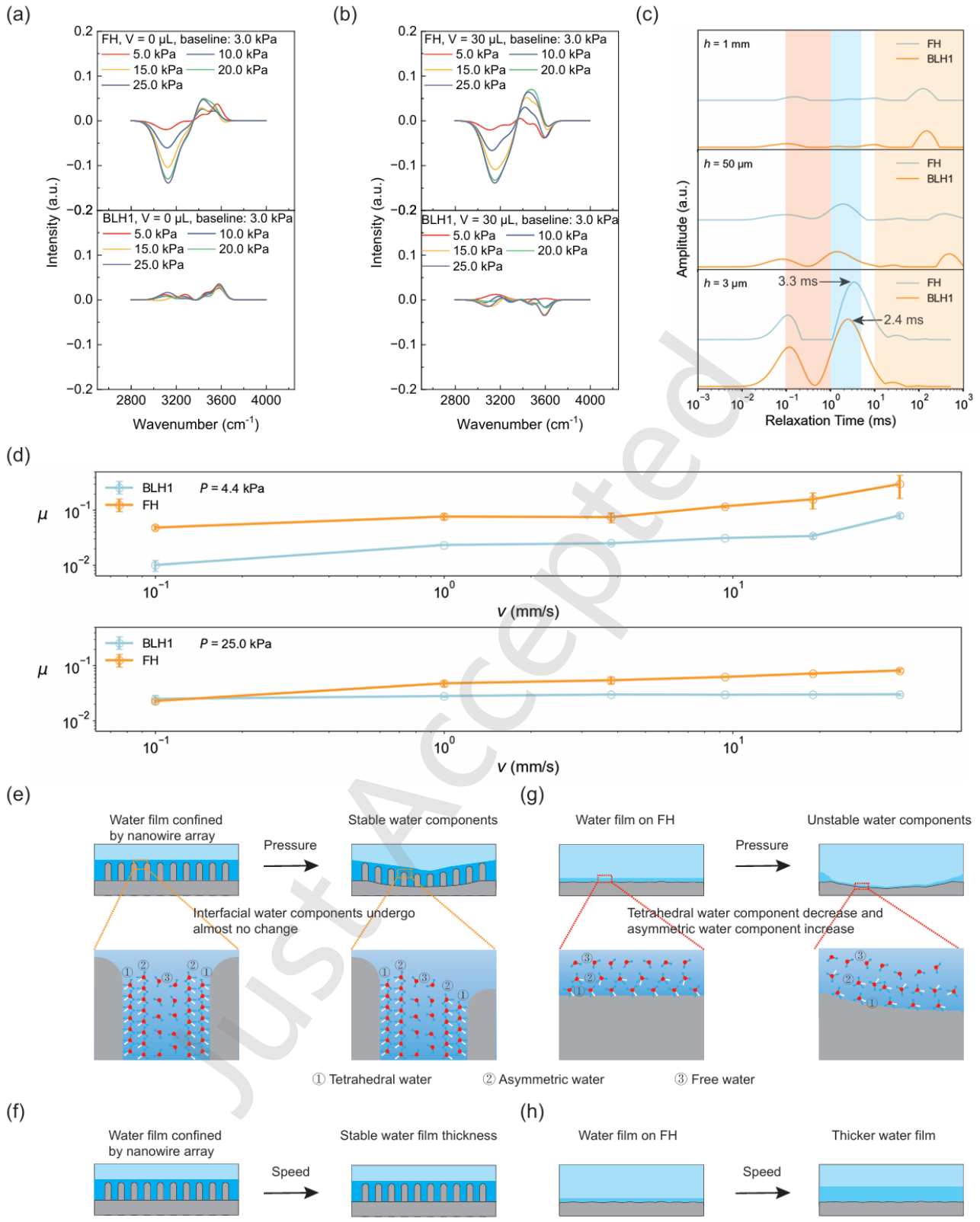

Fig 3. Performance of interfacial water under increasing pressures at microscale. (a) Comparison of components change of FH and BLH1 under pressures (baseline: 3.0 kPa; water volume 0 μL). (b) Comparison of components change of FH and BLH1 under pressures (baseline: 3.0 kPa; water volume 30 μL). (c) LF-NMR of BLH1 and FH at thicknesses of 1 mm, 50 μm, and 3 μm (to eliminate hydrogel

internal water effects). (d) COF of BLH1 and FH at increasing velocities and under 4.4 and 25.0 kPa. (e) Schematic of interfacial water on BLH1 surfaces under pressures: confined water film remains stable; components unchanged. (f) Schematic of thickness change of confined water film on BLH1 surfaces at higher speed: stable water film thickness. (g) Schematic of interfacial water on FH surfaces under pressures: unstable water film; tetrahedral water ratio decreases; asymmetric water ratio increases. (h) Schematic of thickness change of water film on FH surfaces at higher speed: thicker water film.

Integrating the macroscopic friction behavior with the microscopic interfacial water structure, the lubrication characteristics of BLH1 and FH can be summarized as follows (Fig. 3d). Within the physiologically relevant range (e.g., 4.4 kPa), the COF of BLH1 remains consistently lower than that of FH across all tested velocities. At the upper end of the experimental range (25.0 kPa), BLH1 and FH exhibit similar COF values at low velocity; however, BLH1 maintains a low COF at higher velocities, whereas the COF of FH increases markedly with velocity. Accordingly, the lubrication mechanism of BLH1 is proposed as illustrated in Fig. 3e and Fig. 3f, in which confined water on BLH1 surface have stability of interfacial water components under increasing pressure, while also confined water can maintain its thickness at higher speed, as a result, BLH1 can maintain low COF at higher velocity. As to FH surfaces (Fig. 3g and Fig. 3h), water on FH surfaces cannot maintain the components stability under increasing pressure, and at higher speed, water film will be thicker and produce more fluid resistance and thus inducing higher COF. Thus, we could conclude that at nanoscale, for example in nanowire confinement, and in hydrodynamic lubrication, increasing ratio of tetrahedral water will result in higher friction, while increasing ratio of asymmetric water will result in higher lubrication. Besides, interfacial water confined by nanowire array has more ratio of asymmetric water and less ratio of tetrahedral water and thus good lubrication under weak pressure.

2.4 Application of BLH in biomedicals

Friction plays a critical role in the performance and comfort of corneal contact lens. When contact lens move across the corneal surfaces and interact with the eyelids during blinking, friction determines the

smoothness of this movement [40,41]. Excessive friction can lead to discomfort, epithelial damage, and an increased risk of inflammation [42-46], while too low friction may compromise lens stability. Optimizing friction is essential to ensure both ocular health and wearing comfort.

A pig eyeball rubbing model was employed to evaluate the potential of BLH as a contact lens material for reducing corneal injury. As illustrated in Fig. 4a, pig eyeballs were fixed on a scaffold and rubbed with BLH1 or FH; water was applied to the corneal surface before each friction test. After rubbing, the corneas were photographed under white light and blue excitation light following fluorescein sodium staining, using a handheld slit lamp (Fig. 4b). During friction, hydrogel will press on cornea and then slide at specific velocity, the edge of hydrogel will inevitably leave imprint due to edge stress and the space between the edge imprint is the friction area. We selected 45.0, 100.0 mN and 0.1, 0.5 mm/s and compared the injury of BLH1 and FH. Fig. 4c, Fig. S10 and Fig. S11 show the results of friction: under physiologically relevant eyelid pressures, cornea wear by BLH show less staining area and less imprint than cornea wear by FH, showing that reducing friction can help protect cornea. Quantitative analysis in Fig. 4d demonstrated the reduction of BLH1 in injury compared with FH. Lower scores represent less jury. Under physiologically relevant eyelid pressures, BLH1 reduce 50%-90% scores than FH, showing less injury than FH. The standard of scores is illustrated in Methods.

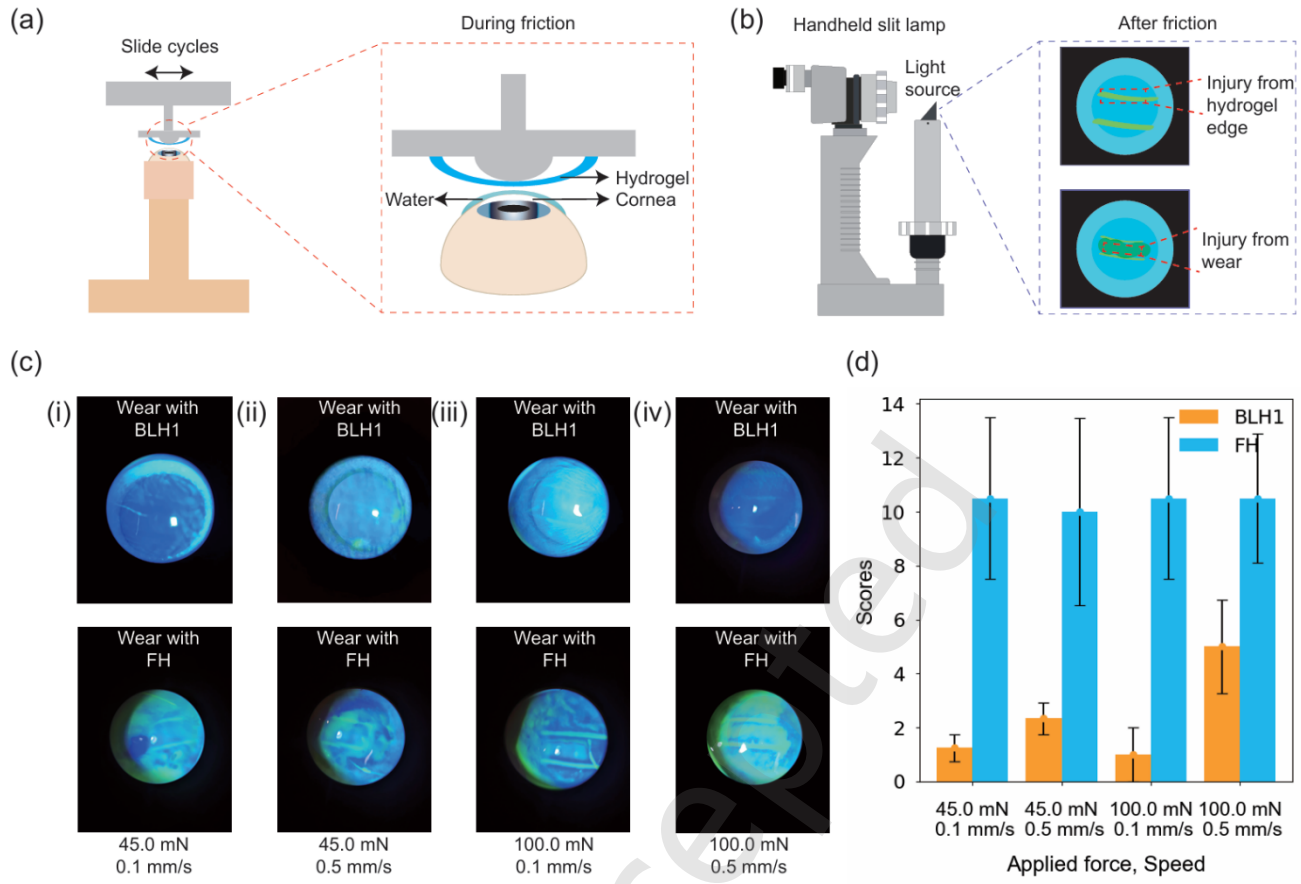

Fig 4. Demonstration of performance of BLH1 and FH in reducing injury on cornea. (a) Illustration of device during friction. (b) Schematics of handheld slit and cornea surfaces after friction and fluorescein sodium staining. (c) Images of cornea rubbed under different conditions: (i) 45.0 mN and 0.1 mm/s, (ii) 45.0 mN and 0.5 mm/s, (iii) 100.0 mN and 0.1 mm/s, (iv) 100.0 mN and 0.5 mm/s. BLH1 outperforms FH under all conditions. (d) Quantitative analysis of fluorescein sodium staining under different conditions. All error bars represent 3 parallel samples.

Besides, we also designed an *in vitro* endoscopic simulation system (Fig. 5a and Fig. 5b) using a transparent acrylic conduit to mimic intestinal lumen conditions. A neodymium magnet simulated the endoscopic camera module, while two ferromagnetic actuators generated controlled magnetic fields for pressure application and motion guidance. The actuators performed reciprocating linear motion at 5.0 mm/s over a 40 mm displacement range. For enhanced visualization, BLH1 and FH were differentially stained with methyl orange and methyl blue, respectively, with dye effects on friction properties confirmed as negligible (Fig. S12). BLH1 and FH share similar Young's modulus of about 2.3 MPa and similar compressive modulus of about 6.0 MPa. (Fig. S13 and Fig. S14). Motion parameters included

actuator displacement (x_0), magnet displacement (x_1), and hydrogel displacement (x_2), which were analyzed at 0.5 s intervals. As is shown in Fig. 5c, BLH1 demonstrated superior interfacial coupling, maintaining synchronous motion between the magnet and hydrogel with minimal hysteresis. In contrast, FH exhibited progressive decoupling from the magnet within 3.0 s, accompanied by significant motion delay relative to actuator movement. Derived parameters Δx_1 ($|x_1 - x_2|$, representing hydrogel-magnet coupling) and Δx_2 ($|x_0 - x_1|$, indicating actuator-magnet synchronization) revealed distinct performance characteristics (Fig. 5d). BLH1-coated systems exhibited lower Δx_1 values and Δx_2 magnitudes compared to FH-coated counterparts, confirming enhanced tribological efficiency.

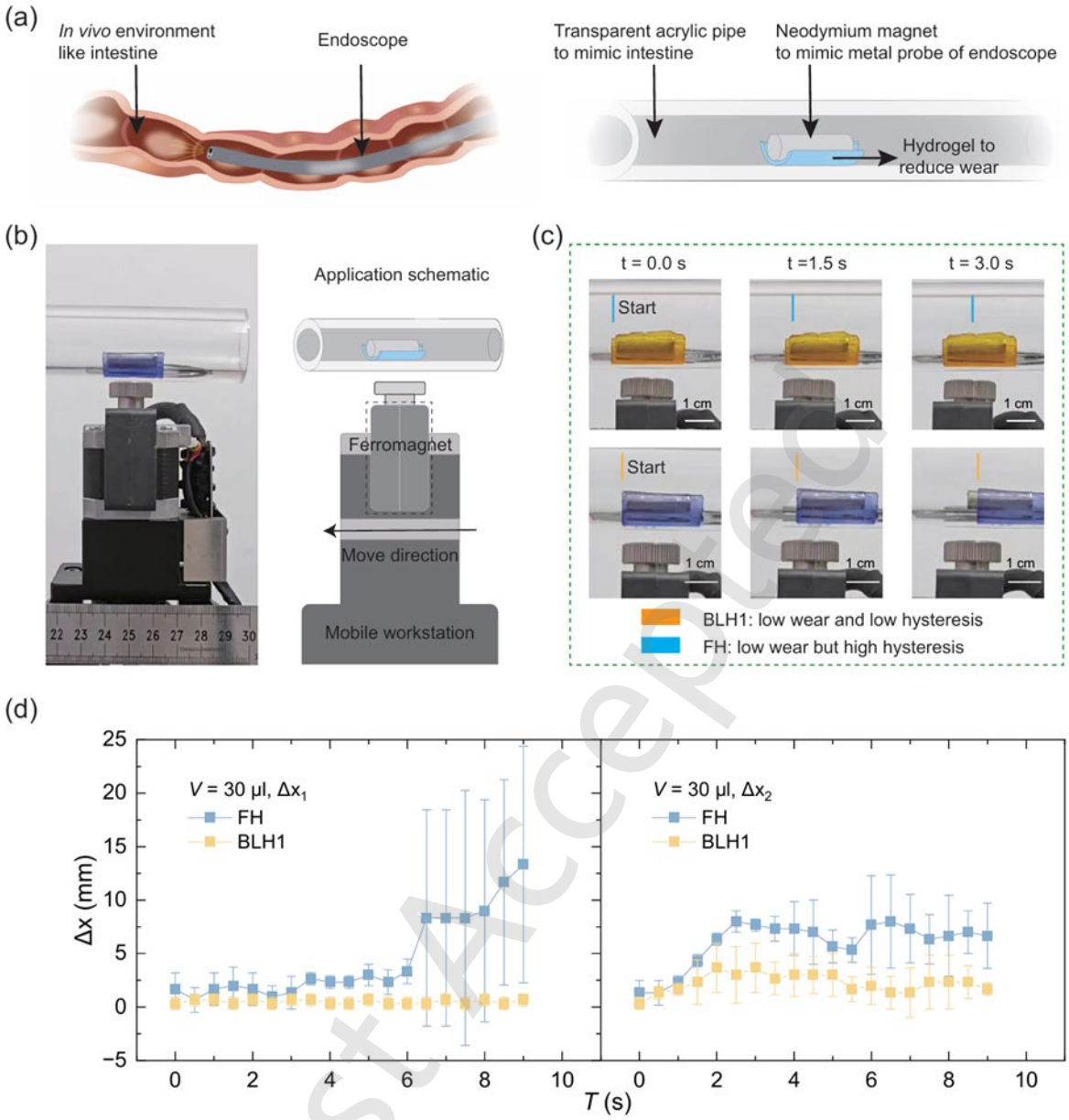

Fig 5. Demonstration of performance of BLH1 and FH as coating materials in an *in vitro* endoscopic simulation system. (a) Schematic of application scenario of BLH1 in endoscope: mimicking intestine (acrylic pipe), metal probe (magnet) with hydrogel for wear reduction. (b) Schematic of BLH1/FH-assisted magnet movement in pipes. (c) Photographs of BLH1-assisted magnet (low wear and low hysteresis) vs FH-assisted (low wear but high hysteresis) at 0, 1.5 and 3.0 s. (d) Data plots of quantitative analysis of magnet displacement. x_0 is ferromagnetic blocks displacement, x_1 is neodymium magnet displacement and x_2 is hydrogel displacement. $\Delta x_1 = |x_1 - x_2|$, and $\Delta x_2 =| x_0 - x_1|$. All error bars represent 3 parallel samples.

In all, we can conclude that, compared with FH, BLH has more interfacial water confined by nanowire array and can reduce friction under weak pressure, causing less corneal damage and showing lower motion hysteresis in endoscopic use.

3 Conclusion

In conclusion, we developed bio-inspired hydrogel surfaces with superior lubrication properties under low-pressure conditions. By incorporating nanowire arrays to modulate interfacial water structure at the microscale, we achieved a mucin-free lubrication design that minimizes friction and movement hysteresis in liquid environments. Our investigation revealed the relationship between interfacial water components and hydrodynamic lubrication, providing new insights into the lubrication mechanism. Additionally, we demonstrated the potential of this approach as contact lens reducing injury to cornea and coating materials for endoscope metal probes in an in vivo like environment due to high lubrication caused by interfacial water confined by nanowire array. We anticipate that this bio-inspired lubrication strategy can be widely applied to reduce resistance and wear in various low-pressure applications, including medical devices and flexible electronics.

Acknowledgements

The authors are grateful for the financial support of Science Fund for Creative Research Groups of the National Natural Science Foundation of China (No. 22521103) and Xiaomi Young Talents Program

Funding

Science Fund for Creative Research Groups of the National Natural Science Foundation of China (No. 22521103)
Xiaomi Young Talents Program

Author contributions

Y.T. and Y.F. conceived and supervised the project. Y.X.W. designed the experiments and carried out most of the experiments. Y.L.W., P.L. and Z.L. provided technical suggestions and carried out some experiments. Y.X.W. and Y.T wrote the manuscript and all authors discussed the results and commented on the manuscript.

Availability of data and materials

The data that support the findings of this study are available from the corresponding author upon reasonable request.

Competing interests

The authors have no competing interests to declare that are relevant to the content of this article.

References

[1] Qin C, Yang H, Lu Y, Li B, Ma S, Ma Y, Zhou F. Tribology in Nature: Inspirations for Advanced Lubrication Materials. *Adv. Mater.* 2420626 (2025).

[2] Marian M, Berman D, Rota A, Jackson R L, Rosenkranz A. Layered 2D nanomaterials to tailor friction and wear in machine elements—a review. *Adv. Mater. Interfaces.* **9**: 2101622 (2022).

[3] Yuan H, Cui W. The lubricated matter in body. *Prog. Mater. Sci.* 101334 (2024).

[4] Slesarenko V, Pastewka L. The bumpy road to friction control. *Science*. **383**: 150-151 (2024).

[5] Evangelista I, Wencel D, Beguin S, Zhang N, Gilchrist M D. Influence of Surface Texturing on the Dry Tribological Properties of Polymers in Medical Devices. *Polymers*. **15**: 2858 (2023).

[6] Bej R, Haag R. Mucus-Inspired Dynamic Hydrogels: Synthesis and Future Perspectives. *J. Am. Chem. Soc.* **144**: 20137-20152 (2022).

[7] Wang X, Huang J, Guo Z. Overview of the development of slippery surfaces: Lubricants from presence to absence. *Adv. Colloid Interface Sci*. **301**: 102602 (2022).

[8] Gao L, Zhao X, Zhang Y, Yang L, Wang R, Ma Z, Liang Y, Ma S, Zhou F. Bioinspired polysaccharide derivative with efficient and stable lubrication for silicon-based devices. *Biomacromolecules*. **23**: 3766-3778 (2022).

[9] Adibnia V, Olszewski M, Crescenzo G D, Matyjaszewski K, Banquy X. Hydrogel coatings on universal medical devices with water-responsive Janus adhesion and acidity-triggered transformation for adaptive antibacterial treatment and fluorescence diagnosis. *J. Am. Chem. Soc.* **142**: 14843-14847 (2020).

[10] Kumar R, Hussainova I, Rahmani R, Antonov M. Solid lubrication at high-temperatures—A review. *Materials*. **15**: 1695 (2022).

[11] Zhang X, Wang J, Jin H, Wang S, Song W. Bioinspired Supramolecular Lubricating Hydrogel Induced by Shear Force. *J. Am. Chem. Soc.* **140**: 3186-3189 (2018).

[12] Huang J, Cao L, Xue C, Zhou Y, Cai Y, Zhao H, Xing Y, Yu S. Extremely soft, stretchable, and self-adhesive silicone conductive elastomer composites enabled by a molecular lubricating effect. *Nano Lett.* **22**: 8966-8974 (2022).

[13] Peng Y, Serfass C M, Kawazoe A, Shao Y, Gutierrez K, Hill C N, Santos V J, Visell Y, Hsiao L C. Elastohydrodynamic friction of robotic and human fingers on soft micropatterned substrates. *Nat. Mater*. **20**: 1707-1711 (2021).

[14] Yang J, Zhang Y, Liu Z, Huang S, Huang X, Wang Y, Li M, Zheng S, Chen F, Liu J, Tao Y, Wu T, Xu L, Chen H, Jiang L, Xie X. Magnetically actuated multimodal bioelectronic catheter for minimally invasive surgery and sensing. *Nat. Mater*. **24**: 2019-2031 (2025).

[15] Tonge P, Roy A, Patel P, Beall C J, Stoyanov P. Tribological evaluation of lead-free MoS2-based solid film lubricants as environmentally friendly replacements for aerospace applications. *Lubricants*. **10**: 7 (2022).

[16] Feng J, Jin A, Li J, Yu Z, Li J, Liu M, Cao Y, Lin W. Advances in high-strength lubricating hydrogels. *Eur. Polym. J*. **241**, 114390 (2025).

[17] Chatterjee A, Dubey D K, Sinha S K. Effect of loading on the adhesion and frictional characteristics of top layer articular cartilage nanoscale contact: A molecular dynamics study. *Langmuir*. **37**: 46-62 (2020).

[18] Lin W, Klein J. Recent progress in cartilage lubrication. *Adv. Mater*. **33**, 2005513 (2021).

[19] Li Y, Yuan Z, Yang H, Zhong H, Peng W, Xie R. Recent advances in understanding the role of cartilage lubrication in osteoarthritis. *Molecules*. **26**: 6122 (2021).

[20] Lin W, Klein J. Hydration lubrication in biomedical applications: From cartilage to hydrogels. *Acc. Mater. Res*. **3**: 213-223 (2022).

[21] Lin W, Kluzek M, Iuster N, Shimoni E, Kampf N, Goldberg R, Klein J. Cartilage-inspired, lipid-based boundary-lubricated hydrogels. *Science*. **370**: 335-338 (2020).

[22] Liu G, Feng Y, Zhao N, Chen Z, Shi J, Zhou F. Polymer-based lubricating materials for functional hydration lubrication. *Chem. Eng. J*. **429**: 132324 (2022).

[23] Chen Y, Gao M, Chen K, Sun H, Xing H, Liu X, Liu W, Guo H. MXene-Based Pressure Sensor with a Self-Healing Property for Joule Heating and Friction Sliding. *Small*. **20**: 2400593 (2024).

[24] Oogaki S, Kagata G, Kurokawa T, Kuroda S, Osada Y, Gong J P. Friction between like-charged hydrogels—combined mechanisms of boundary, hydrated and elastohydrodynamic lubrication. *Soft Matter*. **5**: 1879-1887 (2009).

[25] Guo W, Zhao L, Qin Z, Wang Y, Zhang H. Bioinspired self-adhesive coating for surface functionalization of medical devices with lubrication and antibacterial properties. *Friction*. **13**: 9440926 (2025).

[26] Feldhof M, Schlatterer R, Strahl F, Garthe J, Prévost S, Schmidt S, Karg M, Balzer B N, Hartmann L. Highly Branched Sulfated Glycopolymers as Mucin Mimetics. *J. Am. Chem. Soc.* **147**: 32698-32709 (2025).

[27] Singh A, Corvelli M, Unterman S A, Wepasnick K A, McDonnell P, Elisseeff J H. Enhanced lubrication on tissue and biomaterial surfaces through peptide-mediated binding of hyaluronic acid. *Nat. Mater.* **13**: 988-995 (2014).

[28] Pitenis A A, Urueña J M, Hormel T T, Bhattacharjee T, Niemi S R, Marshall S L, Hart S M, Schulze K D, Angelini T E, Sawyer W G. Corneal cell friction: Survival, lubricity, tear films, and mucin production over extended duration in vitro studies. *Biotribology*. **11**: 77-83 (2017).

[29] Choudhury A, Dey M, Dixit H N, Feng J J. Tear-film breakup: The role of membrane-associated mucin polymers. *Phys. Rev. E.* **103**: 013108 (2021).

[30] Seo J, Byun W Y, Alisafaei F, Georgescu A, Yi Y S, Giordano M M, Shenoy V B, Lee V, Bunya V Y, Huh D. Multiscale reverse engineering of the human ocular surface. *Nat. Med.* **25**: 1310-1318 (2019).

[31] Zhang J, Su Y, Wu J, Wang H. Recent advances in ocular lubrication. *Friction*. **12**: 1929-1954 (2024).

[32] Lievens C W, Rayborn E. Tribology and the ocular surface. Clin. *Ophthalmol*. 973-980 (2022).

[33] Pitenis A A, Urueña J M, Schulze K D, Nixon R M, Dunn A C, Krick B A, Sawyer W G, Angelini T E. Polymer fluctuation lubrication in hydrogel gemini interfaces. *Soft Matter.* **10**: 8955-8962 (2014).

[34] Chau A L, Rosas J, Degen G D, Månsson L K, Chen J, Valois E, Pitenis A A. Aqueous surface gels as low friction interfaces to mitigate implant-associated inflammation. *J. Mater. Chem. B.* **8**: 6782-6791 (2020).

[35] Azimi G, Dhiman R, Kwon H, Paxson A T, Varanasi K K. Hydrophobicity of rare-earth oxide ceramics. *Nat. Mater.* **12**: 315-320 (2013).

[36] Chen L, Qian L. Role of interfacial water in adhesion, friction, and wear—A critical review. *Friction*. **9**: 1-28 (2021).

[37] Fellows A P, Puhan D, Casford M T L, Davies P B. Understanding the lubrication mechanism of poly (vinyl alcohol) hydrogels using infrared nanospectroscopy. *J. Phys. Chem. C*. **124**: 18091-18101 (2020).

[38] Li W, Wang P, Xu X, Xing T, Zhou G. Use of low-field nuclear magnetic resonance to characterize water properties in frozen chicken breasts thawed under high pressure. *Eur. Food Res. Technol.* **239**: 183-188 (2014).

[39] Tan M, Lin Z, Zu Y, Zhu B, Cheng S. Effect of multiple freeze-thaw cycles on the quality of instant sea cucumber: Emphatically on water status of by LF-NMR and MRI. *Food Res. Int.* **109**: 65-71 (2018).

[40] Nečas D, Kulíšek V, Štěpán P, Ondreáš F, Čípek P, Angeles G H, Vrbka M. Friction and lubrication of eye/lens/lid interface: the effect of lubricant and contact lens material. *Tribo. Lett.* **71**: 118 (2023).

[41] Chiang J, Tajbakhsh Z, Wolffsohn J. The clinical impact of contact lens wear on neural structure and function of the cornea. *Clin. Exp. Optom.* **4**: 408-418 (2025).

[42] Kato H, Yokoi N, Watanabe A, Komuro A, Sonomura Y, Sotozono C, Kinoshita S. Relationship between ocular surface epithelial damage, tear abnormalities, and blink in patients with dry eye. *Cornea*. **38**: 318-324 (2019).

[43] Ahn H, Ji Y, Jun I, Kim T, Lee H, Seo K. Effects of meibomian gland dysfunction and aqueous deficiency on friction-related disease. *Ocul. Surf.* **26**: 295-299 (2022).

[44] Veernala I, Jaffet J, Fried J, Mertsch S, Schrader S, Basu S, Vemuganti G K, Singh V. Lacrimal gland regeneration: The unmet challenges and promise for dry eye therapy. *Ocul. Surf.* **25**: 129-141 (2022).

[45] Ma F, Feng J, Liu X, Tian Y, Wang W, Luan F, Wang Y, Yang W, Bai J, Zhang Y, Tao Y. A synergistic therapeutic nano-eyedrop for dry eye disease based on ascorbic acid-coupled exosomes. *Nanoscale*. **15**: 1890-1899 (2023).

[46] Zhang Y, Zhou T, Wang K, Luo C, Chen D, Lv Z, Han H, Yao K. Corneal Mucin-Targeting Liposome Nanoplatforms Enable Effective Treatment of Dry Eye Diseases by Integrated Regulation of Ferroptosis and Inflammation. *Adv. Sci.* **12**: 2411172 (2025).

Yi Xiao Wang received his Bachelor's degree from Shandong University in 2021. Now he is a doc toral candidate at the Technical Institute of Physics and Chemistry, Chinese Academy of Sciences. His research interest focuses on the design and fabrication of super-lubricity materials.

Ye Tian received her PhD degree from the Institute of Chemistry, Chinese Academy of Sciences in 2011. Now she is a full professor in the Technical Institute of Physics and Chemistry. Her research interest focuses on biomi metic multi-dimensional interfacial materials with super spreading.